Insights on the extraordinary tolerance to alcohols of Fe-N-C cathode catalysts in highly performing direct alcohol fuel cells

D. Sebastián,[a] A. Serov,[b] I. Matanovic,[b,c] K. Artyushkova,[b] P. Atanassov,[b] A.S. Aricò,[a] and V. Baglio*[a]*

*[a] Istituto di Tecnologie Avanzate per l'Energia "Nicola Giordano" (ITAE), Consiglio Nazionale delle Ricerche (CNR), Via Salita S. Lucia sopra Contesse 5, 98126, Messina (Italy). * E-mail: baglio@itae.cnr.it*

*[b] Department of Chemical and Biological Engineering and Center for Micro-Engineered Materials, Farris Engineering Center, University of New Mexico, Albuquerque, NM 87131 (USA). * E-mail: plamen@unm.edu*

[c] Theoretical Division, Los Alamos National Laboratory, Los Alamos, NM 87545 (USA)

Abstract

Direct alcohol fuel cells (DAFCs) represent the best alternative to batteries for portable and auxiliary power units application due to the high energy density of short chain alcohols. Currently, the utilization of the best platinum group metal (PGM) cathode catalysts is limited, not only by a high cost and scarce resources, but also by the inefficient oxygen reduction reaction (ORR) when permeated alcohols adsorb on the catalytic active sites. In this work, a highly active Fe-N-C catalyst derived from the pyrolysis of nicarbazin (a nitrogen charge transfer organic salt) and an iron precursor has been investigated to get insights on the extraordinary tolerance to the presence of alcohols (methanol and ethanol) of such a PGM-free catalyst. Density functional theory (DFT) calculations demonstrate for the first time that Fe-N_4 and Fe-N_2C_2 active sites preferentially adsorb oxygen with much higher energy than methanol, ethanol and ethanolic compounds (0.73-1.16 eV stronger adsorption), while nitrogen-carbon related sites (pyridinic and graphitic nitrogen) are much less selective towards ORR. Half-cell electrochemical characterization showed that the Fe-N-C catalyst overcomes Pt ORR activity in acidic medium with methanol or ethanol concentrations as low as 0.01 M. The feasibility of DAFCs operation based on high methanol (up to 17 M) and ethanol (up to 5 M) concentration thanks to the utilization of Fe-N-C cathode catalyst is demonstrated. A new strategy is proposed for DAFCs where using Pt only at the anode and Fe-N-C at the cathode allows extending the device energy density compared to PGM-based catalysts at both electrodes.

Keywords: Electrocatalysis; oxygen reduction reaction; alcohol tolerance; fuel cell; density functional theory.

1. Introduction

High energy density systems capable of producing electricity from renewable sources are demanded by society to overcome the problems associated with the production and use of current power supply devices [1,2]. The ever-increasing market of small portable electronic devices (1-50 W) such as smartphones, laptop computers, tablets, drones, global positioning systems (GPS), modules, as well as auxiliary power units for telecommunication, wireless devices and campers (<1.5 kW), together with the need for environmentally friendly and sustainable processes and products, have stimulated the search for improved power supply systems [3]. Direct alcohol fuel cells (DAFCs) perfectly match the demanding requirements of energy density (pure methanol and ethanol have 6100 and 8040 mWh g^{-1}, respectively), good power density and easy and fast recharging [4].

Despite the great efforts addressed to developing oxygen reduction reaction (ORR) catalysts [5,6], there are yet important barriers to overcome for the commercialization of DAFCs, such as their high cost (more than 50% derived from the use of noble metal catalysts) [7] and the limited power density at high alcohol concentration [4]. Optimum alcohol concentration is found in the range of 1-2 M, which implies dilution with water and consequently much lower energy density and water management requirements [3,8]. DAFC systems capable of working with high fuel concentration would mean a significant step forward towards high capacity electrical systems. Unfortunately, the higher the alcohol concentration, the worse the influence of permeated fuel on performance due to the crossover effect [9,10]. In the case of ethanol as fuel, the breakdown of C-C bond is additionally a relevant concern to increase efficiency [11].

Platinum group metal-free (PGM-free) catalysts based on transition metal – nitrogen – carbon material system (M-N-C where M = Fe, Co, Mn, etc.) have shown a very high activity towards the ORR [12–14]. Other than this, a much less investigated property of the M-N-C catalysts is their extraordinary tolerance to the presence of alcohols like methanol or ethanol. Since their application in DAFC cathodes has been much less studied compared to H_2-fed polymer electrolyte fuel cell activities [15,16], very little is known about the causes for the high selectivity to ORR in the presence of alcohols. Recent papers from our groups indicate an enormous advantage of employing Fe-N-C in terms of selectivity to ORR [17–19], but the causes are still unclear as well as the consequences for the implementation in high energy systems based on fuel cells.

Herein, we investigate the ORR selectivity of a Fe-N-C catalyst derived from the pyrolysis of a nitrogen-containing charge transfer organic salt: nicarbazin (*N,N'-bis(4-Nitrophenyl)urea compound with 4,6-dimethyl-2-pyrimidinone*) and Fe salt, denoted as Fe-NCB. Accordingly, computational calculations on adsorption energies are carried out for the first time to assess the basis of alcohol tolerance properties in such PGM-free catalyst, being further corroborated by electrochemical experiments.

2. Methodology and materials

2.1. Catalyst synthesis

The Fe-NCB catalyst was synthesized by a previously described method.[20] First, a calculated amount of silica (Cab-O-Sil® M5P, surface area 125 $m^2\ g^{-1}$, dried at 85°C) was dispersed in water using a high energy ultrasound bath. Then, a suspension of nicarbazin (Nicarbazin, Sigma-Aldrich) in water was added to the silica dispersion and sonicated for 20 minutes in an ultrasound bath. Finally, a solution of iron nitrate ($Fe(NO_3)_3 \cdot 9H_2O$, Sigma-

Aldrich) in water was added to the silica-nicarbazin (SiO_2-NCB) dispersion and ultrasonically treated for 1 hour (the total metal loading on silica was calculated to be ~26 wt%). The viscous gel of silica and Fe-NCB was dried overnight at 85°C. The obtained solid was ground to a fine powder in an agate mortar and then subjected to heat treatment (HT). The general conditions of HT were ultrahigh purity (UHP) nitrogen (flow rate of 100 mL min^{-1}) and 10°C min^{-1} temperature ramp rate. The temperature and duration of HT were selected as 950 °C and 30 minutes, respectively. After pyrolysis, silica was leached using 25 wt% HF overnight. Finally, the Fe-NCB catalyst was washed with deionized water until neutral pH was achieved and then dried at 85°C. A second HT was performed at 950°C, 45 min in reactive (NH_3) atmosphere.

2.2. Physico-chemical characterization

X-ray photoelectron spectroscopy (XPS) analyses were acquired on a Kratos Axis Ultra DLD X-ray photoelectron spectrometer using an Al Kα source monochromatic operating at 150 W with no charge compensation. Survey and high-resolution spectra were acquired at pass energies of 80 eV and 20 eV, respectively from three areas from sample. Acquisition time for survey spectra was 2 minutes, for C1s and O1s spectra - 5 minutes, for N1s and Fe2p – 30 minutes. Data analysis and quantification were performed using CasaXPS software. A linear background subtraction was used for quantification of C1s, O1s and N1s spectra, while a Shirley background was applied to Fe2p spectra. Sensitivity factors provided by the manufacturer were utilized. A 70% Gaussian/30% Lorentzian line shape was utilized in the curve-fit of N1s.

2.3. Computational methods

Electronic structure calculations were performed using generalized gradient approximation (GGA) to density functional theory (DFT) with the Perdew-Burke-Ernzerhof (PBE) functional [21,22] and projector augmented-wave pseudopotentials [23,24] as implemented in Vienna Ab initio Software Package (VASP) [25–28]. The electronic energies were calculated using 3x3x1 k-point Monkhorts-Pack [29] mesh and tetrahedron method with Blöchl corrections [30]. Plane-wave basis cut-off was set to 700 eV. Extended surfaces were modelled using super-cells with the dimensions of 17.04 Å x 17.04 Å, γ = 60̊ and a vacuum region of 20 Å. Active sites of the Fe-NCB catalyst were modelled by removing one C atom from the graphene in the case of graphitic nitrogen sites and two adjacent C atoms in the case of Fe-N_4, Fe-N_2C_2, and pyridinic sites, respectively. The resulting vacancy in the case of graphitic nitrogen was filled with one nitrogen atom, while in the case of Fe-N_4, Fe-N_2C_2, and pyridinic site, internal edges are substituted with four or two nitrogen atoms, respectively. The resulting structures were further coordinated to Fe atom to obtain Fe-N_4 and Fe-N_2C_2 structures. During the optimization, all atoms were allowed to relax until the convergence in energy was $1 \cdot 10^{-5}$ eV. The lattice was kept fixed at the DFT optimized value for graphene, with C-C distance of 1.42 Å. Adsorption energies (ΔE_{ad}) of oxygen, methanol, ethanol, acetic acid, and acetaldehyde were calculated using the following formula:

$$\Delta E_{ad} = E_{surface+ad} - \left[E_{surface} + E_{ad}\right]$$

where $E_{surface+ad}$ is the energy of a corresponding species adsorbed on the Fe-N-C surface, $E_{surface}$ is the energy of the clean surface, and E_{ad} is the energy of oxygen, methanol, ethanol, acetic acid, and acetaldehyde in the gas phase. In each case we considered several

possible adsorption positions/configurations and the results reported in this work correspond to the most preferable adsorption orientation.

2.4. Electrochemical characterization

Electrochemical studies were carried out in a three-electrode cell at room temperature. The working electrode consisted of a thin film catalyst deposited on a glassy carbon disk (5 mm) of rotating disk electrode (RDE). The catalytic layer was deposited following this recipe: first preparing 3 mg mL^{-1} ink by sonicating the catalyst in isopropyl alcohol/water (3/1, v/v) solution and Nafion® (Ion Power, 5 wt%). A calculated volume of this ink was deposited onto the RDE to the desired mass loading according to previous works [17,31] (600 μg cm^{-2} for the Fe-NCB catalyst, 15 wt% Nafion®; and 50 μg Pt cm^{-2} for the 40 wt% Pt/C commercial catalyst, Johnson Matthey, 30 wt% Nafion®). 0.5 M H_2SO_4 was used as base electrolyte, the reference electrode was a mercury/mercury sulphate ($Hg|Hg_2SO_4$, sat. K_2SO_4) electrode and a high surface graphite rod was used as counter electrode. A Metrohm Autolab potentiostat/galvanostat was used to carry out the electrochemical measurements. Linear sweep voltammetry curves were carried out in the potentiostatic mode with a scan rate of 5 mV s^{-1} and at rotation rates from 100 rpm to 2500 rpm. The tolerance of the catalysts to the presence of methanol and ethanol was evaluated by adding increasing aliquots of the alcohols to the base electrolyte, saturated with oxygen, for concentrations from 0.001 M to 2 M. The ORR response in the presence of alcohols was evaluated at a rotation speed of 1600 rpm.

2.5. Direct alcohol fuel cell tests

Cathode electrodes were prepared by spraying a catalytic ink on a commercial hydrophobic gas diffusion layer (GDL-LT, E-TEK). The catalyst ink was prepared sonicating the catalyst in an isopropyl alcohol/water mixture (3/1, v/v) and Nafion® solution. Cathode electrodes were prepared using the PGM-free catalyst (Fe-NCB) with loading values in the interval 4-8 mg cm^{-2}. The Nafion® content in the catalytic layer was 45 wt% in all cases. For comparison purposes, a cathode based on commercial 40 wt% Pt/C (Johnson Matthey) was prepared following the same procedure (1 mg Pt cm^{-2}, 33 wt% Nafion®). Anode electrodes based on PtRu black (Pt:Ru 1:1, Johnson Matthey) were prepared according to the procedure described in a previous report [18]. The catalytic layer was composed of 85 wt% catalyst and 15 wt% Nafion® ionomer, spread onto a commercial gas diffusion layer (GDL-HT, E-TEK). The noble metal (Pt+Ru) loading at the anode was in the interval from 1 to 4 mg cm^{-2}. Membrane electrode assemblies (MEAs) were assembled by a hot-pressing procedure at 130 °C and 30 kg-f cm^{-2} during 10 minutes, and subsequently installed in a 5 cm^2 fuel cell test fixture (Fuel Cell Tech., Inc.). In the various MEAs, the membrane was maintained constant: a Nafion® 115 membrane (~130 μm) was used as the solid electrolyte. The cell hardware was connected to a Fuel Cell Tech., Inc. test station. In the case of single cell polarization experiments, aqueous methanol (from 1 M to 17 M) or aqueous ethanol (from 1 M to 5 M) solutions were pre-heated at the same temperature of the cell and fed to the anode chamber of the DAFC through a peristaltic pump; oxygen, pre-heated at the same temperature of the cell (100% relative humidity), was fed to the cathode. Reactant flow rates were 2 and 100 mL min^{-1} for alcohol/water mixture and oxygen stream, respectively. The cell temperature was measured by a thermocouple embedded in the cathodic graphite plate, close to the MEA.

142 Steady-state galvanostatic polarization experiments in DAFC configuration were performed
143 with an Agilent electronic load at various conditions of temperature (from 30°C to 110°C)
144 and alcohol concentration (from 1 M to 17 M). Alcohol cross-over was determined by
145 electrochemical methods, using ad hoc MEAs based on Pt/C cathode, as described
146 elsewhere [32]. Durability tests were carried out in the potentiostatic mode at 0.3 V and
147 90°C feeding 5 M methanol (DMFC) or 3 M ethanol (DEFC) to the anode and fully
148 humidified oxygen to the cathode under the same conditions of polarization experiments.
149 Every 10 hours a polarization curve was registered to assess the performance variation
150 with time.

151 ## 3. Results and discussion

152 ### 3.1. Tolerance to the presence of alcohols

153 **Figure 1** shows the effect of methanol and ethanol concentration on the ORR polarization
154 curves (half-cell configuration) for the Fe-NCB catalyst (red lines in the figure). A
155 commercial Pt/C catalyst (grey lines in the figure) is included for the sake of comparison.
156 The effect of three alcohol concentrations (2, 20, 200 mM) is depicted. Negative current
157 values account for the ORR, whereas positive oxidation currents account for the oxidation
158 reaction of alcohols (methanol, MOR, or ethanol, EOR). It is noteworthy that the presence
159 of either methanol or ethanol does not significantly affect the ORR polarization curve of
160 the Fe-NCB catalyst, even with concentrations as high as 200 mM. As shown in the
161 **supplementary information**, the high tolerance to the presence of both alcohols is
162 maintained even at concentrations achieving 2 M, with less than 10 mV shift of the ORR
163 half-wave potential (**Figures S1a and S1b**).
164

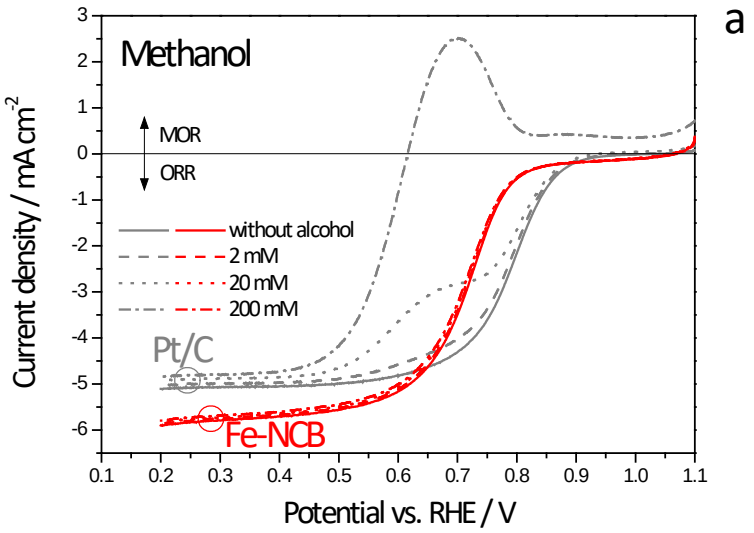

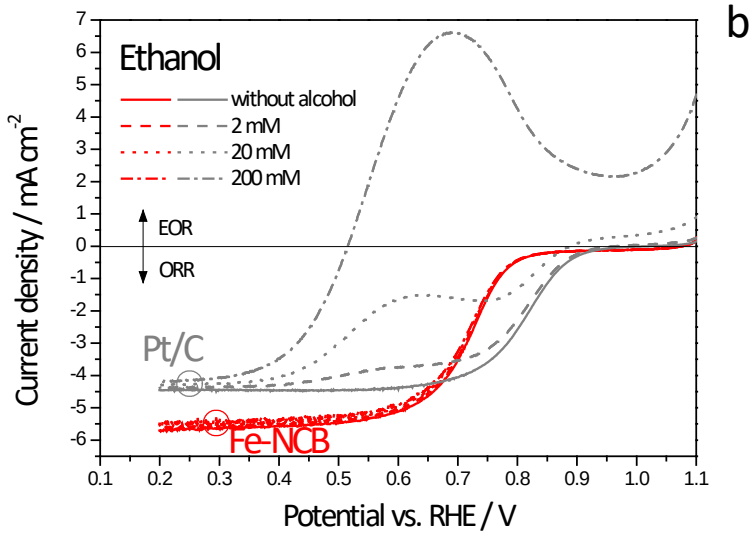

Fig. 1 Oxygen reduction reaction (ORR) activity for the PGM-free catalyst (Fe-NCB) and a commercial Pt/C catalyst and effect of (a) methanol and (b) ethanol concentration on the polarization response in RDE half-cell configuration. O_2-saturated 0.5 M H_2SO_4, 1600 rpm, 600 µg cm^{-2} (Fe-NCB) and 50 µg cm^{-2} Pt (Pt/C).

Whereas, the commercial Pt/C catalyst exhibits a dramatic variation of the ORR behaviour (**Figure 1**), because it is also a good catalyst for the MOR and EOR, and strongly chemisorbs alcohols [33]. Indeed, methanol and ethanol compete with oxygen for the Pt active sites as a function of voltage and alcohol concentration. The ORR half-wave potential is, in the case of the Pt/C catalyst, shifted up to 300 mV (2 M methanol, **Figure S1c**) and 430 mV (2 M ethanol, **Figure S1d**) to more negative values. These experiments indicate a very good ORR

activity of Fe-NCB in the presence of both methanol and ethanol, the so-called good tolerance to the presence of alcohols. The whole set of polarization curves are included in the **Figure S1** of the **supplementary information**.

A proper analysis of the advantageous application of the PGM-free formulation with respect to the classical Pt/C catalyst can be more easily understood by analysing **Figure 2**. The potential gap between the Fe-NCB and the Pt-based catalysts is represented as a function of the alcohol concentration in the electrolyte, under identical conditions. The half-wave potential, i.e. the potential at half the diffusion limiting current, is an excellent indicator of ORR activity of a catalyst and is commonly used to assess catalytic performance in the mixed catalytic-diffusion region. A positive gap must be interpreted as favourable conditions for Fe-NCB, whereas a negative gap means that Pt/C utilization is more advantageous for the ORR. At very low alcohol concentration, there is about 75 mV gap indicating that Pt is yet more active for the ORR than Fe-NCB. Whereas, when the alcohol concentration approaches 10^{-2} mol L^{-1}, the gap is reduced to zero and, afterwards, at higher concentration, the gap dramatically increases over 100 mV, favourable for the use of the PGM-free catalyst. It is also interesting to remark that the potential gap is higher in the case of ethanol compared to methanol at equal concentrations.

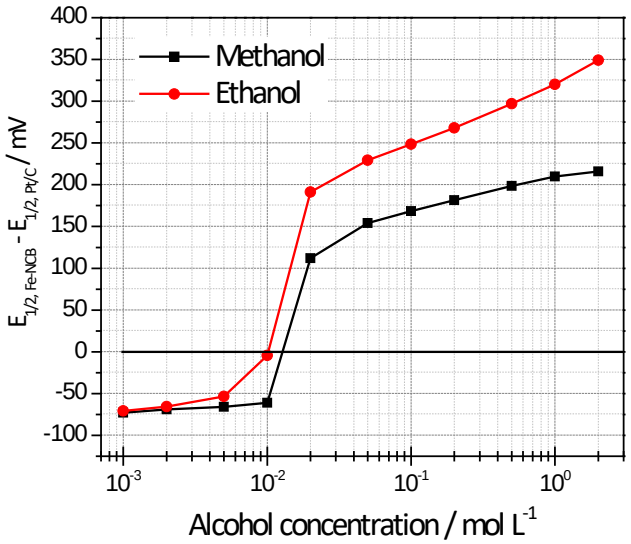

Fig. 2 ORR half-wave potential ($E_{1/2}$) gap between the Fe-NCB catalyst and a commercial Pt/C catalyst as a function of alcohol concentration in the electrolyte (O_2-saturated 0.5 M H_2SO_4).

The results in half-cell configuration point out that, above a certain concentration of crossovered alcohol at the cathode compartment, the utilization of Fe-NCB catalyst is preferred because the catalytic sites remain highly active for the oxygen reduction with a negligible effect of the presence of alcohols.

3.2. Adsorption of organic species calculated by DFT

The concerns on alcohol crossover in DAFCs are not only related to the loss of fuel from the anode to the cathode through the membrane (lowering the fuel efficiency), but to the dramatic decay of cathode performance due to the adsorption of alcoholic species on Pt catalytic active sites, hindering the adsorption of oxygen [9,10]. Density functional theory (DFT) calculations were carried out, aimed at better investigating the relative importance of the adsorption of different organic molecules on the ORR catalytic activity. For the Fe-NCB catalyst, four species were taken into account as active sites for the ORR according to the literature [34–37]: Fe-N_4, Fe-N_2C_2, pyridinic nitrogen and graphitic nitrogen. The

possible adsorbates, other than molecular oxygen, were considered to be methanol (CH_3OH), ethanol (CH_3CH_2OH), acetic acid (CH_3COOH) and acetaldehyde (CH_3CHO). Methanol and ethanol are the fuels that permeate from the anode to the cathode side. **Figure 3** shows, as an example, a representation of the structures regarding the Fe-N_4 and the Fe-N_2C_2 sites as well as the preferred orientation for the adsorption of oxygen and the two alcohol molecules. In the ethanol oxidation reaction (EOR), CO_2 is not the only oxidation product, but it is a minor subproduct together with acetic acid and acetaldehyde [38]. These two organic compounds can also permeate through the membrane to the cathode compartment [39] and, even if in much smaller concentration than ethanol, they may adsorb on the catalyst active sites, contributing to the decrease of cell performance.

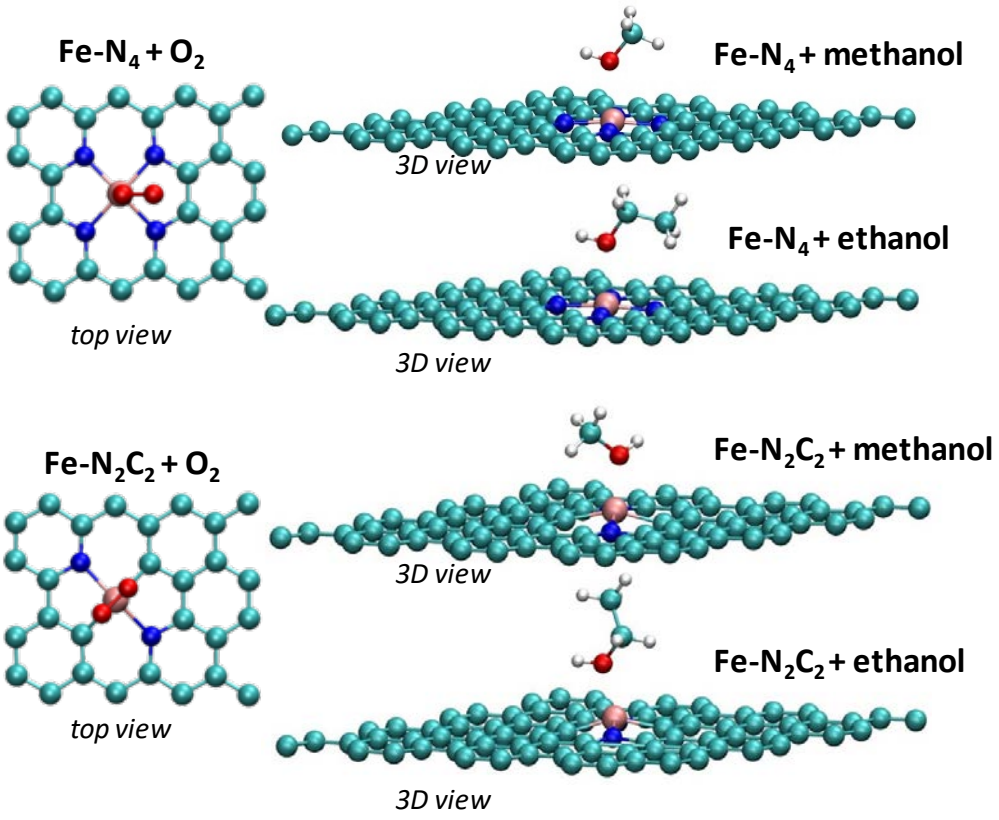

Fig. 3 DFT optimized structures of Fe-N_4 and Fe-N_2C_2 sites with adsorbed methanol and ethanol. Atoms belonging to one unit cell are shown (C cyan, N blue, Fe pink, O red, H white).

Table 1 summarizes the theoretical calculations on adsorption energies associated to the different molecules on the above cited ORR active sites, calculated as described in the experimental section.

According to DFT, the adsorption energies of molecular oxygen on Fe-N_4 and Fe-N_2C_2 are -1.01 and -1.68 eV, respectively, quite more negative than those calculated on graphitic nitrogen (-0.13 eV) and pyridinic nitrogen (-0.06 eV). Thus, the adsorption of oxygen occurs preferably on Fe-based active sites compared to nitrogen-carbon moieties (**Figure S2**).

Methanol and ethanol adsorb significantly more weakly than oxygen on Fe-N_4 and on Fe-N_2C_2 sites (**Figures S3 and S4**). The net difference in adsorption energy between oxygen and the alcohols is 1.16 eV in the case of Fe-N_2C_2 sites, where oxygen preferably adsorbs. On Fe-N_4 sites, this difference is slightly lower (0.79 eV). It appears that methanol and ethanol are not adsorbed on graphitic nitrogen (barely 0.01 eV, **Figure S5**), so even if the adsorption of oxygen is weaker than on Fe-based sites, alcohols seem to not compete with oxygen, although the adsorption energy is quite lower compared to Fe-based active sites.

Table 1 Adsorption energies (eV) of different species on Fe-N_4, Fe-N_2C_2, pyridinic nitrogen (N pyrid), graphitic nitrogen (N graph) sites as obtained using DFT with PBE functional and comparison with platinum.

	Fe-N_4	Fe-N_2C_2	N pyrid	N graph	Pt
O_2	-1.01	-1.68	-0.06	-0.13	-0.44 to -0.81 [40]
CH_3OH	-0.22	-0.52	-0.28	+0.01	-0.28 [41]
CH_3CH_2OH	-0.17	-0.57	-0.27	-0.01	-0.23 to -0.81 [42]
CH_3COOH	-0.25	-0.68	-0.41	-0.03	+0.17 [42]
CH_3CHO	-0.28	-0.61	-0.15	-0.03	-0.35 [42]

Interestingly, the case of pyridinic nitrogen (**Figure S6**) is quite different; there is a preferable adsorption of methanol (-0.28 eV) and ethanol (-0.27 eV) on this active site compared to molecular oxygen (-0.06 eV). This means that an ORR catalyst characterized by only pyridinic nitrogen active sites would not be tolerant to the presence of alcohols, whereas Fe-N_4, Fe-N_2C_2 and, in a lower extent, graphitic nitrogen, would exhibit a high tolerance to alcohols and a high selectivity towards the ORR.

Regarding the effect of eventual traces of acetic acid or acetaldehyde, the adsorption energies of both ethanolic residues on the ORR active sites are also summarized in **Table 1**. The adsorption energies of these molecules are even more negative than those of ethanol on Fe-N_4 (-0.25 eV and -0.28 eV), Fe-N_2C_2 (-0.68 and -0.61 eV) and graphitic nitrogen (-0.03 eV). Still, there is a preferential adsorption of oxygen on Fe-based sites. In the case of pyridinic nitrogen, the adsorption of of ethanolic residues is stronger than that of oxygen, especially for acetic acid (-0.41 eV), adsorbing much stronger than ethanol.

From a cross analysis of the electrochemical results in half-cell configuration concerning alcohol tolerance properties and the DFT computational calculations on adsorption energies, it appears that the Fe-NCB catalyst herein investigated might be characterized by a significant density of active sites of the Fe-N_2C_2 or the Fe-N_4 types.

The interaction of platinum with oxygen, methanol, ethanol, and other small molecules has been extensively studied in previous works. For example, adsorption energies calculated for oxygen on Pt(111) surface range between -0.44 and -0.81 eV depending on the DFT functional [40,43,44]. While it was found that acetic acid does not chemisorb on the Pt(111) surface, the adsorption energies calculated for methanol, ethanol and acetaldehyde range between -0.23 and -0.81 eV [42,45]. Therefore, it is expected that the interaction of alcohols with the Pt surface will be comparable or slightly less stronger than

the interaction of oxygen, indicating that the blocking effect by these organic molecules could be much less pronounced on Fe-NCB catalyst than on a platinum one.

3.3. DMFC and DEFC performance analysis

The Fe-NCB catalyst was evaluated at the cathode side of a DMFC and a DEFC. A wide range of operating conditions and electrode loadings were investigated to best cover the potential applicability of the PGM-free formulation on DAFCs. In particular, high alcohol concentrations were studied aimed at getting insights on the suitability of Fe-NCB cathode catalyst in high energy density DAFCs. The effect of electrode catalyst loadings on the polarization and power density curves is shown in **Figure 4** at high alcohol concentration (10 M methanol and 5 M ethanol). In DMFC (**Figure 4a**), two cathode loadings (Fe-NCB, 4 and 8 mg cm^{-2}) and two anode loadings (PtRu, 1 and 4 mg cm^{-2}) were tested on the basis of our previous experience [17,31,46]. There is an increase of performance in terms of maximum power density from 50 to 60 mW cm^{-2} when increasing the PtRu loading at the anode from 1 to 4 mg cm^{-2}. However, it appears that a high Fe-NCB loading (8 mg cm^{-2}) influences negatively the polarization curve at current densities higher than 200 mA cm^{-2}. A thicker cathode electrode might cause water saturation and flooding, hindering the diffusion of oxygen to the active sites [47]. The open circuit potential (OCP) was 0.8 V for the MEAs with 1 mg PtRu cm^{-2} at the anode and slightly higher (0.82 V) for a loading of 4 mg PtRu cm^{-2}. Despite the relatively high OCP, polarization curves exhibit a sharp decrease of voltage at low current density coming from the contribution of the sluggish kinetics of both anodic and cathodic reactions, especially the alcohol electro-oxidation at the anode, causing significant overpotentials. The polarization and power density curves of a Pt-cathode-based MEA are also included in **Figure 4**. The highest impact of the high tolerance

294 to alcohols of the Fe-NCB catalyst is clearly seen at the low current density zone. The OCP
295 for the MEA with the Pt/C cathode is as low as 0.5 V, which means a loss of voltage of
296 about 300 mV compared to the Fe-NCB based MEAs. The low performance in the activation
297 controlled region for the Pt/C cathode is clearly a result of the high methanol crossover
298 influencing oxygen reduction active sites availability. As the current increases, the
299 performance of the Fe-NCB cathode-based MEAs becomes lower than that of the Pt/C,
300 which may be attributed to a combination of two effects: a thicker cathode electrode,
301 hindering oxygen diffusion; and the well-known decrease of crossovered methanol with
302 current. However, the voltage efficiency in the high current density region is very low (< 0.2
303 V) and is not of practical interest.
304 In DEFC configuration, two anode catalyst loadings were tested (PtRu, 2 and 4 mg cm^{-2}).
305 **Figure 4b** shows the results obtained at high ethanol concentration (5 M). An increase of
306 performance is observed using higher PtRu loading. It must be pointed out that even
307 though PtRu is known to be very active for the EOR [48], it is not the very best formulation
308 to attain high performances. Indeed, better performances have been reported using PtSn
309 anode catalysts [49,50]. Nevertheless, we preferred to adopt this commercial catalyst at
310 the anode for sake of comparison, which could be transferred to a more performing MEA
311 with more active anode catalysts.

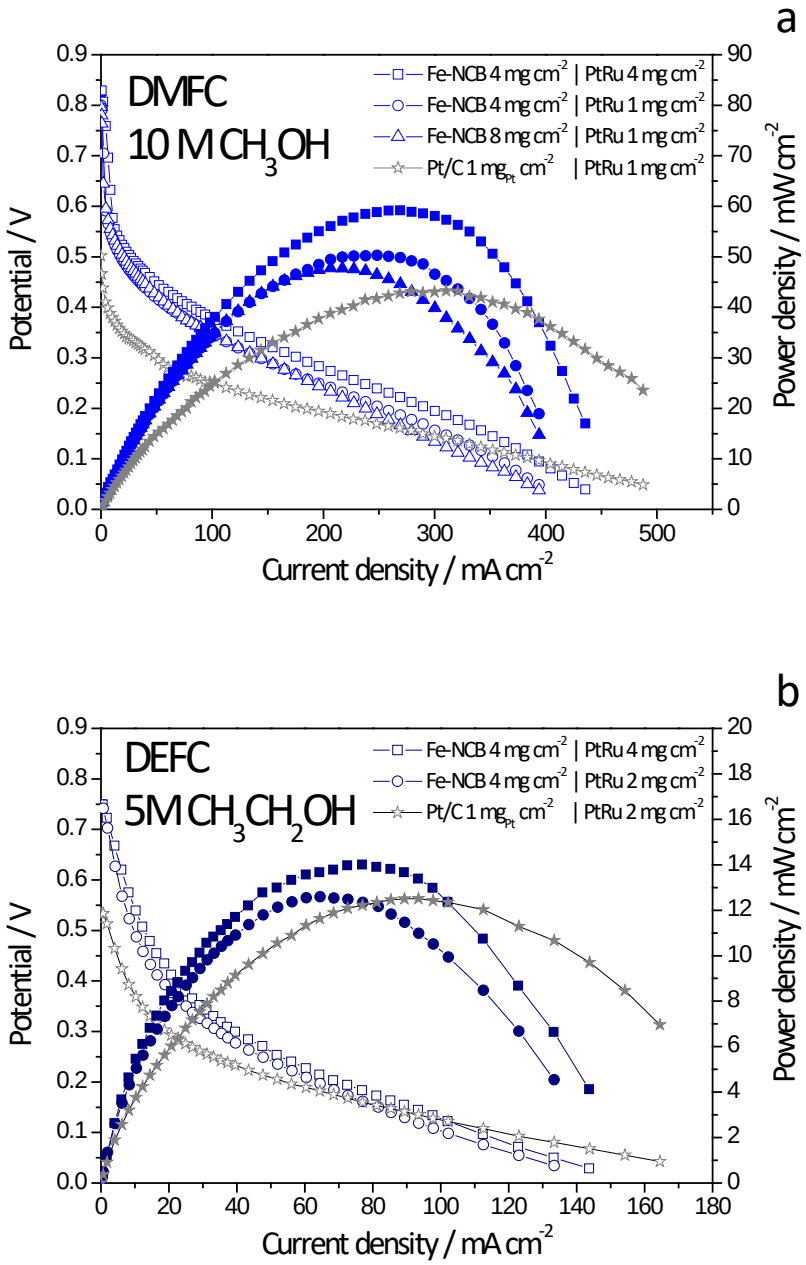

Fig. 4 Effect of electrodes composition and loading on the performance of (a) DMFC and (b) DEFC. The legend shows cathode (left) and anode (right) loadings. Operating conditions: 90°C, 10 M methanol (a) or 5 M ethanol (b) at the anode (2 mL min^{-1}) and fully humidified oxygen at the cathode (100 mL min^{-1}). Membrane: Nafion® 115.

A bar chart showing the maximum power density values in DAFCs is represented in **Figure 5** on the basis of fuel concentration, cell temperature and catalysts loadings. An MEA based on Pt/C cathode is included for comparison. Regarding Fe-NCB MEAs, a moderate increase of power density with the methanol concentration in DMFC is observed as a general trend

(**Figure 5a**). Instead, the opposite trend is exhibited in DEFC configuration, with a slight decrease of performance when feeding high ethanol concentration (**Figure 5b**). The MEAs based on Pt/C cathode show a larger decrease of power density with alcohol concentration compared to Fe-NCB cathodes (DMFC and DEFC). It is remarkable that using Fe-NCB cathode configuration is much better than Pt/C working with high alcohol concentration, even if the maximum power density represents a condition for relatively high current density and low voltage, in which alcohol crossover effects are less detrimental compared to high voltage operation. The advantageous use of highly tolerant PGM-free cathode is further accentuated under higher voltage operation, i.e. high energy efficiency. This is derived from the negligible effect of alcohol concentration on the polarization curves at high voltage (**Figures S7** and **S8**), attributed to the high tolerance to the presence of alcohols of the Fe-NCB catalyst.

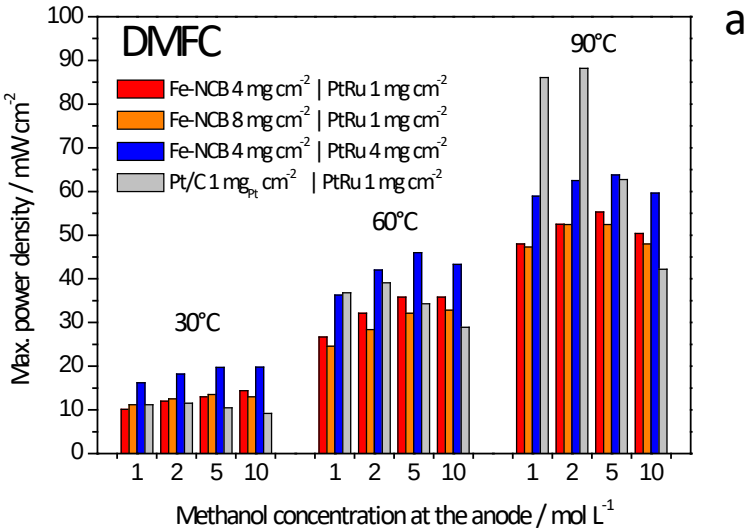

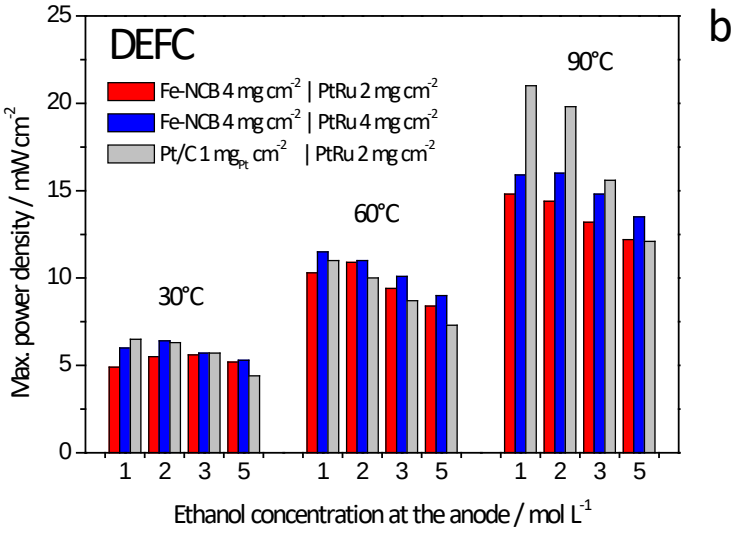

Fig. 5 Maximum power densities in (a) DMFC and (b) DEFC configurations as a function of electrode loadings, operating temperature and alcohol concentration at the anode.

Table 2 summarizes some important features concerning the performance analysis carried out in this investigation. As described in the introduction section, one of the main disadvantages of highly concentrated fuel solutions is the consequent increase of permeation rate to the cathode compartment exacerbated by the swelling of the polymer which increases its porosity [10]. Just to illustrate this, crossover experiments were carried out using *ad hoc* MEAs based on the same Nafion® membrane, and Pt/C and PtRu catalysts at the cathode and anode sides, respectively. The crossover equivalent current, associated to the oxidation of permeated alcohol at Pt/C at the cathode, is a good indication of this well-known phenomenon [51]. A variation of methanol molarity from 1 M to 10 M (10-fold) results in an increase of methanol crossover current from 118 to 591 mA cm^{-2} (5-fold). In the case of ethanol, even if it is not completely oxidized to CO_2 at the cathode, an increase of concentration from 1 M to 5 M (5-fold) leads to an increase of the equivalent crossover current density from 70 to 183 mA cm^{-2} (2.6-fold). The effect of crossover on cell performance is clearly deduced from the variation of cell potential (E) as summarized in

Table 2. Using the conventional Pt/C cathode, the cell potential decreases 110 mV (DMFC) and 90 mV (DEFC) when increasing the alcohol concentration from the lowest to the highest tested levels. Whereas, the cells equipped with the Fe-NCB cathode show only a decrease of 20 mV (DMFC) and 30 mV (DEFC). This is a corroboration of the high tolerance of the Fe-NCB catalyst to the presence of alcohols and alcoholic residues, as discussed in previous sections, under more realistic conditions. As a consequence, a high tolerance of the Fe-NCB cathode catalyst allows operating at high fuel concentrations while maintaining a high performance.

Table 2 Fuel energy density*, crossover of methanol (CH_3OH) and ethanol (C_2H_5OH) through Nafion® 115 membrane (60°C) and effect on cell potential (E at 10 mA cm^{-2} and 60°C) for the most performing MEAs.

Fuel molarity	Fuel energy density* / mWh g^{-1}	Crossover equivalent current / mA cm^{-2}	E for the Fe-NCB based MEA / V	E for the Pt/C based MEA / V
1 M CH_3OH	194	118	0.52	0.51
2 M CH_3OH	391	205	0.52	0.47
5 M CH_3OH	1003	413	0.51	0.43
10 M CH_3OH	2097	591	0.50	0.40
1 M C_2H_5OH	385	70	0.46	0.44
2 M C_2H_5OH	781	104	0.46	0.40
3 M C_2H_5OH	1187	140	0.45	0.37
5 M C_2H_5OH	1960	183	0.43	0.35

** In the case of ethanol, full conversion to CO_2 is considered. For further information regarding the influence of EOR selectivity on the fuel energy density, please see **Figure 6** and **Table S1** of the **supporting Information**.*

The fuel energy density of both methanol and ethanol is also reported in **Table 2** on the basis of alcohol concentration in water. It is important to remark that, even if pure ethanol (8040 mWh g^{-1}) presents a higher energy density than pure methanol (6100 mWh g^{-1}), the

inefficient oxidation of the former to CO_2 giving acetaldehyde and acetic acid reduces significantly the practical fuel energy density as illustrated in **Figure 6** (it can be even 83% lower if full conversion to acetaldehyde occurs). The selectivity of ethanol oxidation to CO_2, acetic acid and acetaldehyde relies on several factors like anode composition (PtSn, PtRu, etc.), operating temperature, alcohol concentration and voltage/current, among others. Some works report the effect of such parameters on product distribution in DEFCs, using PtRu at the anode [48,52,53], like in the MEAs of the present investigation. In any case, it is clear from the energy density values of **Table 2** that using high alcohol concentration in water is mandatory for prolonged operation of DAFCs.

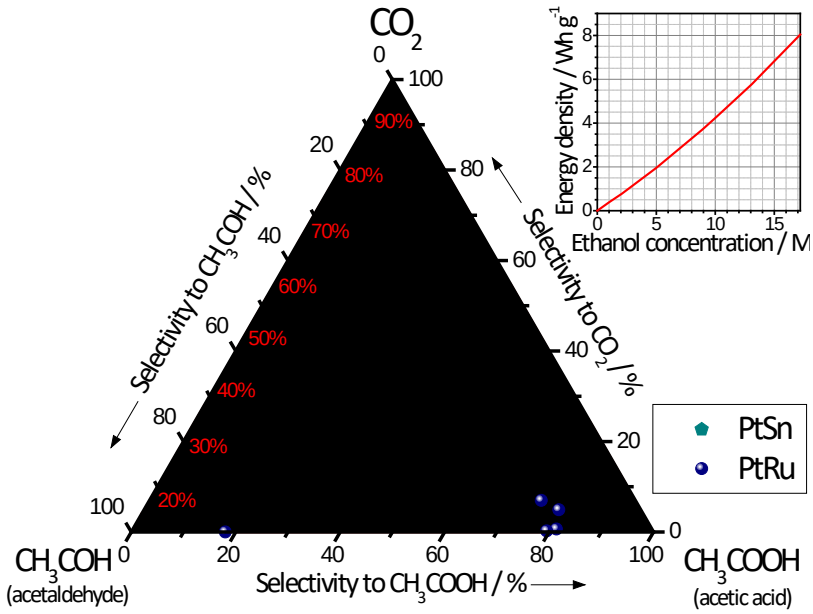

Fig. 6 Fuel energy density diagram as a function of EOR selectivity to CO_2, acetic acid and acetaldehyde. Data for PtRu and PtSn from refs. [48,54,55,52,53]. Red lines indicate the energy content percentage, where 100% represents full conversion to CO_2. Upper-right corner graph: dependence of energy density for 100% conversion to CO_2 with ethanol concentration in water.

DMFC polarization and power density curves were also recorded at very high methanol concentration (17 M, 3888 mWh g^{-1}) and high temperature (110°C), as depicted in **Figure 7**. This is a condition in which methanol is very close to the stoichiometric concentration with

water (17.1 M). The Pt/C cathode-based MEA shows a very low OCP of 0.45 V. In consequence, the entire polarization curve is significantly affected by the low potential in the activation controlled zone (low current density), performing 26 mW cm^{-2} as maximum power density. It is noteworthy that the two MEAs based on Fe-NCB cathodes exhibit a very high OCP (0.76-0.78 V) despite the high methanol concentration at the anode and the high cell temperature. As a matter of fact, the maximum power densities reach 41 and 58 mW cm^{-2} for the MEAs (Fe-NCB cathode) based on low and high loaded PtRu anode, respectively. The higher power density of the Fe-NCB based MEAs is ascribed to the better behaviour in the activation controlled zone, directly related to the extraordinary alcohol tolerance properties of the PGM-free catalyst. This fact highlights the importance of searching alcohol tolerant cathode formulations towards highly performing DAFCs in high energy density systems.

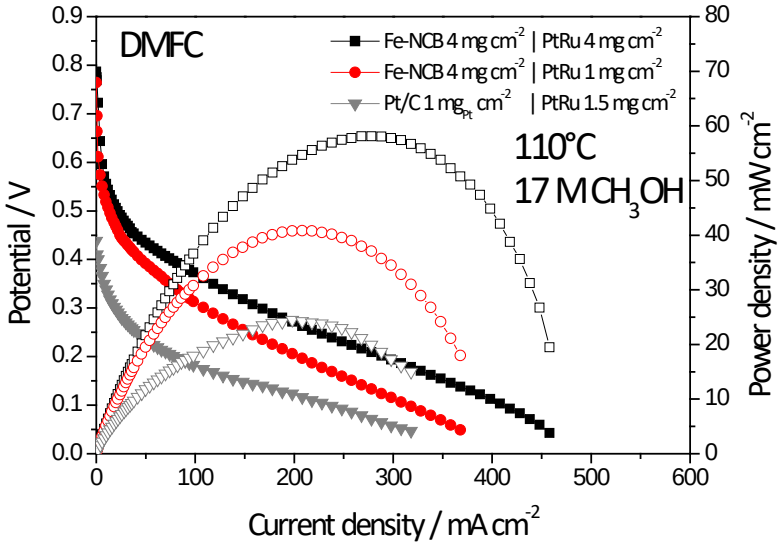

Fig. 7 DMFC polarization and power density curves at high temperature (110°C) and high methanol concentration (17 M) for three MEAs as indicated in the legend (left: cathode; right: anode).

The power density plotted against the fuel energy density is represented in **Figure 8** as a Ragone-like plot for the experiments in DAFCs carried out in the present work. An ideal DAFC-based powering system should provide both high power (W) and high energy (Wh). The results obtained with the Fe-NCB based cathode are indicated by the areas filled with diagonal strips, while the results related to the Pt/C cathode are indicated by the shadowed areas (light orange for DMFC and light yellow for DEFC). The upper line of the areas (red) represents the experiments at 110°C, whereas the lower line (blue) refers to 30°C tests. It must be pointed out here that the cost of an MEA is highly influenced by the amount of platinum in the electrodes, being the most expensive component in a large-scale production process. Thus, the maximum power density normalized by the total amount of Pt offers a very good idea of the cost-efficiency of the DAFC system.

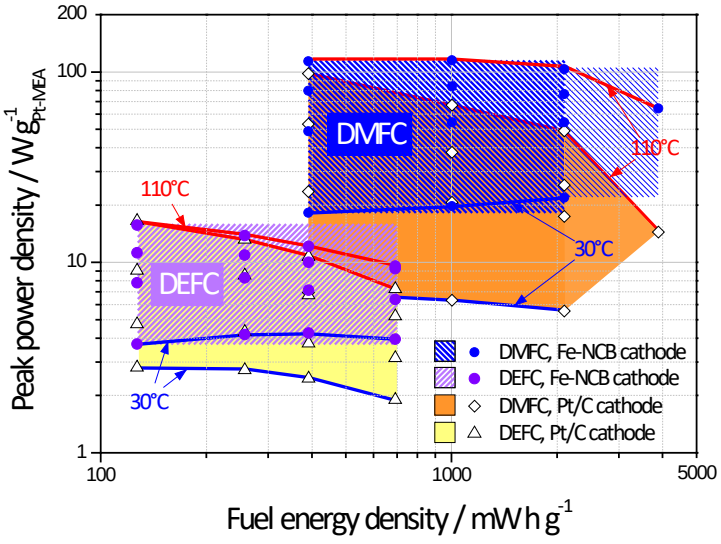

Fig. 8 Ragone-like plot of the DMFC and DEFC experimental results and the fuel energy density according to alcohol concentration. In the case of DEFC, the energy density has been calculated considering EOR energy efficiency of 33%, in line with previous publications [54].

It is deduced from **Figure 8** that a great advantage is gained with the implementation of the Fe-NCB catalyst at the cathode, especially for systems based on high energy density of the fuel (top right area of the figure). A remarkable difference is observed in terms of peak power density (W $g_{Pt\text{-}MEA}^{-1}$) among the two MEA configurations, above all considering that the graph is plotted in double-logarithmic scale. At low temperature (30°C), close to ambient, both DMFC and DEFC performances are significantly enhanced when using the Fe-NCB cathode. The improvement is even larger operating with high fuel energy density. At high temperature (110°C), the highest differences are found when feeding the cell with high alcohol concentration. For example, producing 100 mW $g_{Pt\text{-}MEA}^{-1}$ in a DMFC with a Pt-cathode MEA is constrained to operate at 110°C and methanol concentration not higher than 2M (391 mWh g^{-1}), whereas using the Fe-NCB cathode allows operating at the same temperature but with 10 M methanol (2097 mWh g^{-1}), meaning more than 5-fold increase in energy content (i.e. 5-fold longer duration of the fuel reservoir). Similar conclusions can be extracted by analyzing DEFC data. From these results, it appears that a good strategy for the commercialization of DAFCs is using noble metals only at the anode side (in combination with other cheaper ad-metals like Ru or Sn) and highly tolerant PGM-free catalysts (M-N-C) at the cathode electrode.

3.4. Durability investigation

Durability tests were carried out on fresh MEAs with the Fe-NCB catalyst at the cathode side and PtRu at the anode (**Figure 9**). They consisted of potentiostatic/chronoamperometric curves at 0.3 V, keeping the cell temperature at 90°C and feeding 5 M methanol in DMFC configuration (**Figure 9a**) or 3 M ethanol in the DEFC experiment (**Figure 9b**).

The variation of performance with time of an MEA in a DAFC relies on several factors including cathode, anode and membrane degradation phenomena. In particular, the degradation processes occurring at the cathode side are known to be accelerated by high temperature, high cathode potential, low pH, and high oxygen/water concentration.

In DMFC (**Figure 9a**), the current density shows initially a rapid decrease of performance, with a loss of power density of about 2.5 % h^{-1}, and then the degradation is decelerated to about 0.3 % h^{-1}. The average rate of performance loss is 0.67 % h^{-1}. This is higher than the loss of performance of an MEA based on Pt/C under similar conditions (**Figure S9**): 0.45 % h^{-1} [17]. Nevertheless, high temperature post-treatments of Fe-N-C catalysts have been demonstrated to significantly enhance the resistance to degradation at the cathode [46].

In DEFC, the performance variation with time is shown in **Figure 9b**. In the initial 3 hours of the experiment a rapid decrease of performance was registered, followed by a smoother decay. The first 10 hours account for a loss rate of 3.5 % h^{-1}. Then, the degradation of the MEA is much slower, with a rate of about 0.2 % h^{-1} at the end of the test (similar to DMFC rate). The variation of performance with time in the case of DEFC is similar to that obtained for a Pt/C cathode-based MEA under the same conditions (**Figure S9**).

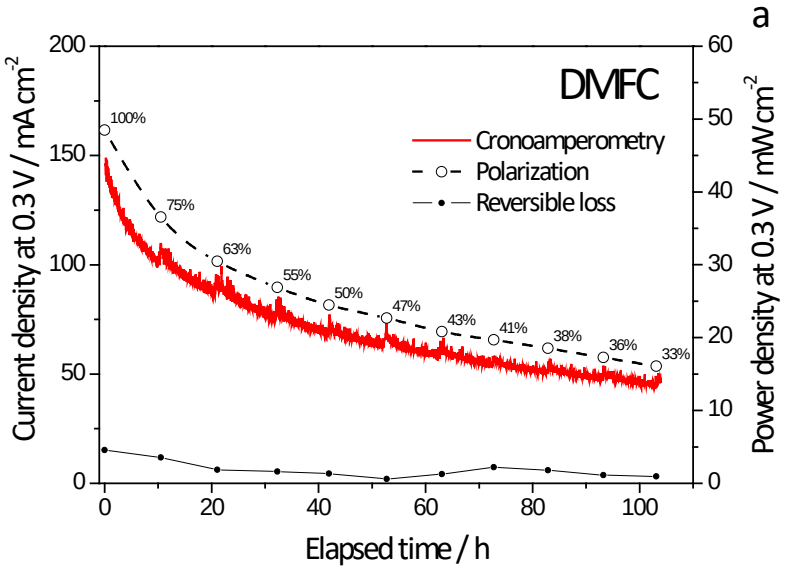

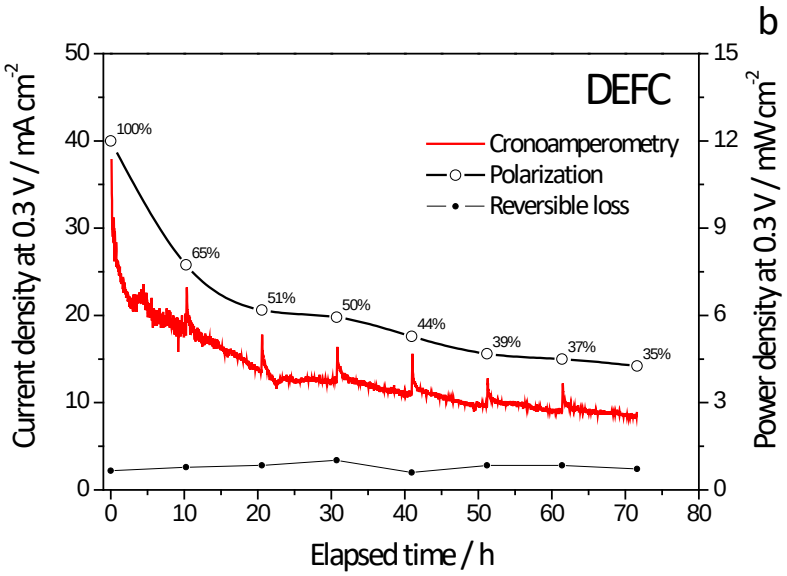

Fig. 9 Durability tests carried out at 0.3 V and 90°C for the Fe-NCB catalyst used at the cathode side. (a) DMFC configuration: 5 M methanol fed to the anode (2 mL min^{-1}) and fully humidified oxygen to the cathode (100 mL min^{-1}), cathode loading: 4 mg Fe-NCB cm^{-2}, anode loading: 1 mg PtRu cm^{-2}. (b) DEFC configuration: 3 M ethanol fed to the anode (2 mL min^{-1}) and fully humidified oxygen to the cathode (100 mL min^{-1}), cathode loading 4 mg Fe-NCB cm^{-2}, anode loading: 2 mg PtRu cm^{-2}. Nafion® 115 membrane. The reversible loss is calculated as the difference of the current densities measured in the polarization curve at 0.3 V and measured in the chronoamperometric curve right after the polarization.

In an attempt to rationalize the contribution of the cathode to the overall performance loss, XPS analyses were carried out on the Fe-NCB electrode after the durability tests and on a fresh electrode for the sake of comparison. The N1s spectra are shown in **Figure 10**. Fresh cathode has typical distribution of nitrogen species with protonated (401.9 eV) and hydrogenated (401 eV) nitrogens being the largest contributors [56]. Graphitic nitrogen contributes to both peaks at 401.9 eV and 403.0 eV. Oxidized nitrogen (NO_x) appears at highest binding energy around 405 eV. The sites that demonstrate highest adsorption of oxygen contribute to lower binding energy range. The peak at 398.5 eV has contribution from pyridinic nitrogen and Fe-N_2C_2 sites, while Fe-N_4 sites contribute to peak at 399.9 eV. It appears that nitrogen speciation barely changes after the durability tests (**Table 3**) with some decrease of protonated and graphitic nitrogen and increase in relative amount of active sites exposed at the surface of catalyst layers. The irreversible performance decay

with time could be thus more related to the degradation of other MEA components in this particular case, like the anode or the membrane. It is well known that Ru is susceptible to leaching out the anode [57].

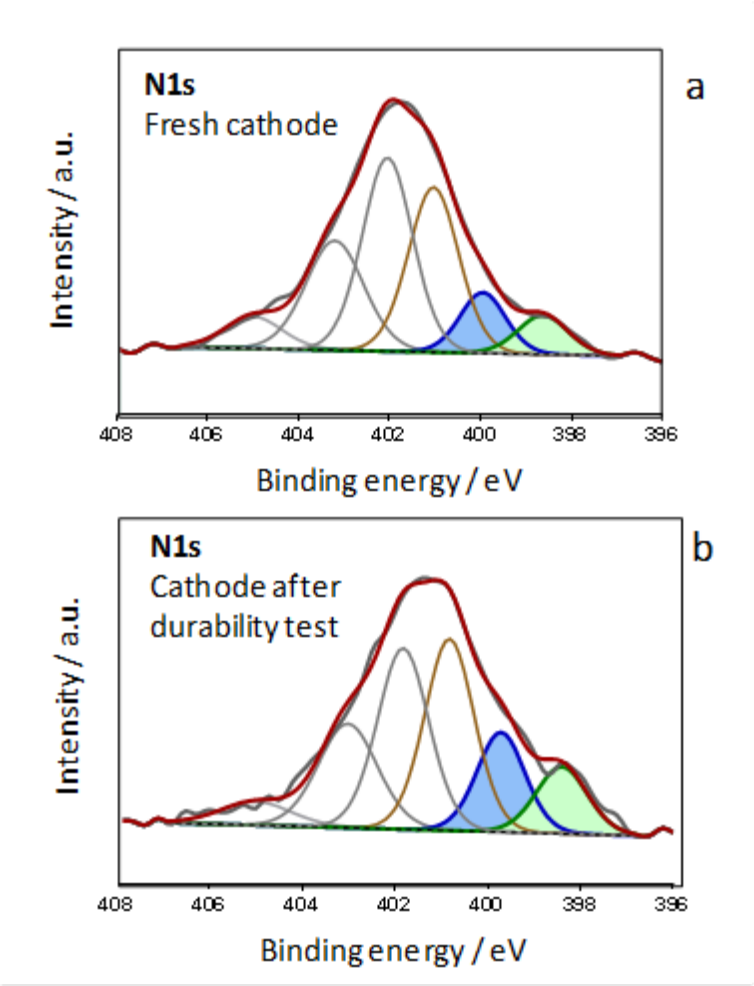

Fig. 10 XPS analyses performed on the cathodic electrode (a) at the beginning of life and (b) at the end of DMFC durability test. Shadowed areas correspond to pyridinic nitrogen (light green) and N-Fe (light blue).

Table 3 N speciation (at%) from XPS analysis of fresh and used electrode (after 100 h in DMFC potentiostatic operation).

	N pyrid	N-Fe	N hydro	N proton	N graph	NO_x
	398.5 eV	399.9 eV	401.0 eV	401.9 eV	403.0 eV	405.0 eV
Fresh	7.1	8.3	25.6	31.7	21.1	6.2
Used	10.4	18.4	21.4	30.1	17.8	2.0

3.5. Outlook

Cost-effective PGM-free catalysts have become of paramount interest for the development of highly efficient and performing power sources like fuel cells. Other than a low cost, these active catalysts exhibit an extraordinary tolerance to some small organic molecules like methanol and ethanol. This property makes them very attractive to solve one of the most important problems concerning direct alcohol fuel cells (DAFCs): low performance when increasing the energy density of the fuel. Insights on the causes of high tolerance for Fe-N-C catalysts indicate the best route towards optimization of DAFCs components, in particular with regard to the best active sites required at the cathode side. The calculations are corroborated with tests in single cell, with performances as high as 60 mW cm^{-2} with high methanol concentration of 10 M (up to 17 M by increasing the temperature). The work indicates that using noble metals only at the anode side is the most convenient strategy for cost-effective and high energy density systems based on DAFCs.

4. Conclusions

The oxygen reduction electrochemical activity of a PGM-free catalyst based on iron – nitrogen – carbon (Fe-N-C) has been investigated in the presence of methanol and ethanol. Computational calculations by DFT demonstrated that Fe-N_4 and Fe-N_2C_2 sites exhibit a significantly stronger adsorption of oxygen compared to alcohols and ethanolic intermediates like acetic acid and acetaldehyde, in contrast to commonly used Pt-based catalysts, which experience competition of alcohols and oxygen for the active sites. The preferred adsorption of oxygen on Fe-N-C catalyst has been proven to positively and greatly influence the behaviour at the cathode of DAFCs. A promising strategy consisting of using noble metals at the anode side and the Fe-N-C catalyst at the cathode side is here

proposed and demonstrated to broaden the energy density of power supply sources based on highly efficient DAFCs.

Acknowledgements

VASP license was provided by Theoretical division, LANL, which is supported by the Office of Science of the U.S. Department of Energy under Contract No. DE-AC52-06NA25396. Computational work was performed using the computational resources of EMSL, a national scientific user facility sponsored by the Department of Energy's Office of Biological and Environmental Research and located at Pacific Northwest National Laboratory, NERSC, supported by the Office of Science of the U.S. Department of Energy under Contract No. DE-AC02-05CH11231, and CNMS, sponsored at Oak Ridge National Laboratory by the Scientific User Facilities Division, Office of Basic Energy Sciences, U.S. Department of Energy. This paper has been designated LA-UR-16-29215.

References

[1] A.S. Aricò, P. Bruce, B. Scrosati, J.-M. Tarascon, W. van Schalkwijk, Nanostructured materials for advanced energy conversion and storage devices., Nat. Mater. 4 (2005) 366–377. doi:10.1038/nmat1368.

[2] S. Chu, A. Majumdar, Opportunities and challenges for a sustainable energy future., Nature. 488 (2012) 294–303. doi:10.1038/nature11475.

[3] X. Li, A. Faghri, Review and advances of direct methanol fuel cells (DMFCs) part I: Design, fabrication, and testing with high concentration methanol solutions, J. Power Sources. 226 (2013) 223–240. doi:10.1016/j.jpowsour.2012.10.061.

[4] X.S. Zhao, M. Yin, L. Ma, L. Liang, C.P. Liu, J.H. Liao, T.H. Lu, W. Xing, Recent advances in catalysts for direct methanol fuel cells, Energy Environ. Sci. 4 (2011) 2736–2753. doi:10.1039/c1ee01307f.

[5] Y. Nie, L. Li, Z. Wei, Recent advancements in Pt and Pt-free catalysts for oxygen reduction reaction., Chem. Soc. Rev. 44 (2015). doi:10.1039/c4cs00484a.

[6] M.D. Allendorf, Oxygen reduction reaction: A framework for success, Nat. Energy. 1 (2016) 16058. doi:10.1038/nenergy.2016.58.

[7] M. Sgroi, F. Zedde, O. Barbera, A. Stassi, D. Sebastián, F. Lufrano, V. Baglio, A. Aricò, J. Bonde, M. Schuster, Cost Analysis of Direct Methanol Fuel Cell Stacks for Mass Production, Energies. 9 (2016) 1008. doi:10.3390/en9121008.

[8] M.Z.F. Kamarudin, S.K. Kamarudin, M.S. Masdar, W.R.W. Daud, Review: Direct ethanol fuel cells, Int. J. Hydrogen Energy. 38 (2013) 9438–9453. doi:10.1016/j.ijhydene.2012.07.059.

[9] S.Q. Song, W.J. Zhou, W.Z. Li, G. Sun, Q. Xin, S. Kontou, P. Tsiakaras, Direct methanol fuel cells : Methanol crossover and its influence on single DMFC performance, Ionics (Kiel). 10 (2004) 458–462. doi:10.1007/BF02378008.

[10] S. Song, W. Zhou, J. Tian, R. Cai, G. Sun, Q. Xin, S. Kontou, P. Tsiakaras, Ethanol crossover phenomena and its influence on the performance of DEFC, J. Power Sources. 145 (2005) 266–271. doi:10.1016/j.jpowsour.2004.12.065.

[11] A. Kowal, M. Li, M. Shao, K. Sasaki, M.B. Vukmirovic, J. Zhang, N.S. Marinkovic, P. Liu, A.I. Frenkel, R.R. Adzic, Ternary Pt/Rh/SnO2 electrocatalysts for oxidizing ethanol to CO2, Nat. Mater. 8 (2009) 325–330. doi:10.1038/nmat2359.

[12] M. Lefèvre, E. Proietti, F. Jaouen, J.-P. Dodelet, Iron-based catalysts with improved oxygen reduction activity in polymer electrolyte fuel cells., Science. 324 (2009) 71–4. doi:10.1126/science.1170051.

566 [13] E. Proietti, F. Jaouen, M. Lefevre, N. Larouche, J. Tian, J. Herranz, J.-P. Dodelet, Iron-based
567 cathode catalyst with enhanced power density in polymer electrolyte membrane fuel cells,
568 Nat. Commun. 2 (2011) 1–6. doi:10.1038/ncomms1427.
569 [14] H.A. Gasteiger, N.M. Marković, Chemistry. Just a dream--or future reality?, Science. 324
570 (2009) 48–9. doi:10.1126/science.1172083.
571 [15] Z. Chen, D. Higgins, A. Yu, L. Zhang, J. Zhang, A review on non-precious metal
572 electrocatalysts for PEM fuel cells, Energy Environ. Sci. 4 (2011) 3167.
573 doi:10.1039/c0ee00558d.
574 [16] F. Jaouen, E. Proietti, M. Lefèvre, R. Chenitz, J.-P. Dodelet, G. Wu, H.T. Chung, C.M.
575 Johnston, P. Zelenay, Recent advances in non-precious metal catalysis for oxygen-reduction
576 reaction in polymer electrolyte fuelcells, Energy Environ. Sci. 4 (2011) 114–130.
577 doi:10.1039/C0EE00011F.
578 [17] D. Sebastián, A. Serov, K. Artyushkova, P. Atanassov, A.S. Aricò, V. Baglio, Performance,
579 methanol tolerance and stability of Fe-aminobenzimidazole derived catalyst for direct
580 methanol fuel cells, J. Power Sources. 319 (2016) 235–246.
581 doi:10.1016/j.jpowsour.2016.04.067.
582 [18] A.S. Aricò, A. Stassi, C. D'Urso, D. Sebastián, V. Baglio, Synthesis of Pd3Co1@Pt/C core-shell
583 catalysts for methanol-tolerant cathodes of direct methanol fuel cells., Chem. - A Eur. J. 20
584 (2014) 10679–84. doi:10.1002/chem.201402062.
585 [19] D. Sebastián, I. Suelves, R. Moliner, M.J.M.J. Lázaro, A. Stassi, V. Baglio, A.S.A.S. Aricò,
586 Optimizing the synthesis of carbon nanofiber based electrocatalysts for fuel cells, Appl.
587 Catal. B Environ. 132–133 (2013) 22–27. doi:10.1016/j.apcatb.2012.11.023.
588 [20] A. Serov, K. Artyushkova, E. Niangar, C. Wang, N. Dale, F. Jaouen, M.-T. Sougrati, Q. Jia, S.
589 Mukerjee, P. Atanassov, Nano-structured non-platinum catalysts for automotive fuel cell

application, Nano Energy. 16 (2015) 293–300. doi:10.1016/j.nanoen.2015.07.002.

[21] J.P. Perdew, K. Burke, M. Ernzerhof, Generalized Gradient Approximation Made Simple, Phys. Rev. Lett. 77 (1996) 3865–3868. doi:10.1103/PhysRevLett.77.3865.

[22] J.P. Perdew, K. Burke, M. Ernzerhof, Generalized Gradient Approximation Made Simple, Phys. Rev. Lett. 78 (1996) 3865–3868. doi:10.1103/PhysRevLett.78.1396.

[23] P.E. Blöchl, Projector augmented-wave method, Phys. Rev. B. 50 (1994) 17953–17979. doi:10.1103/PhysRevB.50.17953.

[24] G. Kresse, From ultrasoft pseudopotentials to the projector augmented-wave method, Phys. Rev. B. 59 (1999) 1758–1775. doi:10.1103/PhysRevB.59.1758.

[25] G. Kresse, J. Hafner, *Ab initio* molecular dynamics for liquid metals, Phys. Rev. B. 47 (1993) 558–561. doi:10.1103/PhysRevB.47.558.

[26] G. Kresse, J. Hafner, *Ab initio* molecular-dynamics simulation of the liquid-metal–amorphous-semiconductor transition in germanium, Phys. Rev. B. 49 (1994) 14251–14269. doi:10.1103/PhysRevB.49.14251.

[27] G. Kresse, J. Furthmüller, Efficiency of ab-initio total energy calculations for metals and semiconductors using a plane-wave basis set, Comput. Mater. Sci. 6 (1996) 15–50. doi:10.1016/0927-0256(96)00008-0.

[28] G. Kresse, J. Furthmüller, Efficient iterative schemes for *ab initio* total-energy calculations using a plane-wave basis set, Phys. Rev. B. 54 (1996) 11169–11186. doi:10.1103/PhysRevB.54.11169.

[29] H.J. Monkhorst, J.D. Pack, Special points for Brillouin-zone integrations, Phys. Rev. B. 13 (1976) 5188–5192. doi:10.1103/PhysRevB.13.5188.

[30] P.E. Blöchl, O. Jepsen, O.K. Andersen, Improved tetrahedron method for Brillouin-zone integrations, Phys. Rev. B. 49 (1994) 16223–16233. doi:10.1103/PhysRevB.49.16223.

[31] D. Sebastián, V. Baglio, A.S. Aricò, A. Serov, P. Atanassov, Performance analysis of a non-platinum group metal catalyst based on iron-aminoantipyrine for direct methanol fuel cells, Appl. Catal. B Environ. 182 (2016) 297–305. doi:10.1016/j.apcatb.2015.09.043.

[32] F. Lufrano, V. Baglio, O. Di Blasi, P. Staiti, V. Antonucci, A.S. Aricò, Design of efficient methanol impermeable membranes for fuel cell applications., Phys. Chem. Chem. Phys. 14 (2012) 2718–26. doi:10.1039/c2cp23477g.

[33] L. Osmieri, R. Escudero-Cid, A.H.A. Monteverde Videla, P. Ocón, S. Specchia, Performance of a Fe-N-C catalyst for the oxygen reduction reaction in direct methanol fuel cell: Cathode formulation optimization and short-term durability, 201 (2017) 253–265. doi:10.1016/j.apcatb.2016.08.043.

[34] S. Kattel, P. Atanassov, B. Kiefer, Stability, Electronic and Magnetic Properties of In-Plane Defects in Graphene: A First-Principles Study, J. Phys. Chem. C. 116 (2012) 8161–8166. doi:10.1021/jp2121609.

[35] S. Kattel, P. Atanassov, B. Kiefer, A density functional theory study of oxygen reduction reaction on non-PGM Fe-Nx-C electrocatalysts., Phys. Chem. Chem. Phys. 16 (2014) 13800–6. doi:10.1039/c4cp01634c.

[36] Y. Jiao, Y. Zheng, M. Jaroniec, S.Z. Qiao, Origin of the electrocatalytic oxygen reduction activity of graphene-based catalysts: A roadmap to achieve the best performance, J. Am. Chem. Soc. 136 (2014) 4394–4403. doi:10.1021/ja500432h.

[37] R.A. Sidik, A.B. Anderson, N.P. Subramanian, S.P. Kumaraguru, B.N. Popov, O2 reduction on graphite and nitrogen-doped graphite: Experiment and theory, J. Phys. Chem. B. 110 (2006) 1787–1793. doi:10.1021/jp055150g.

[38] E. Antolini, Catalysts for direct ethanol fuel cells, J. Power Sources. 170 (2007) 1–12. doi:10.1016/j.jpowsour.2007.04.009.

[39] D.D. James, P.G. Pickup, Effects of crossover on product yields measured for direct ethanol fuel cells, Electrochim. Acta. 55 (2010) 3824–3829. doi:10.1016/j.electacta.2010.02.007.

[40] Z. Šljivančanin, B. Hammer, Oxygen dissociation at close-packed Pt terraces, Pt steps, and Ag-covered Pt steps studied with density functional theory, Surf. Sci. 515 (2002) 235–244. doi:10.1016/S0039-6028(02)01908-8.

[41] A.B. Anderson, H.A. Asiri, Reversible potentials for steps in methanol and formic acid oxidation to CO2; adsorption energies of intermediates on the ideal electrocatalyst for methanol oxidation and CO2 reduction., Phys. Chem. Chem. Phys. 16 (2014) 10587–10599. doi:10.1039/c3cp54837f.

[42] H. a. Asiri, a. B. Anderson, Mechanisms for Ethanol Electrooxidation on Pt(111) and Adsorption Bond Strengths Defining an Ideal Catalyst, J. Electrochem. Soc. 162 (2014) F115–F122. doi:10.1149/2.0781501jes.

[43] M.P. Hyman, J. Will Medlin, Theoretical study of the adsorption and dissociation of oxygen on Pt(111) in the presence of homogeneous electric fields, J. Phys. Chem. B. 109 (2005) 6304–6310. doi:10.1021/jp045155y.

[44] R. Li, H. Li, J. Liu, First principles study of O2 dissociation on Pt(111) surface: Stepwise mechanism, Int. J. Quantum Chem. 116 (2016) 908–914. doi:10.1002/qua.25095.

[45] P. Tereshchuk, J.L.F. Da Silva, Density Functional Investigation of the Adsorption of Ethanol–Water Mixture on the Pt(111) Surface, J. Phys. Chem. C. 117 (2013) 16942–16952. doi:10.1021/jp403352u.

[46] D. Sebastián, A. Serov, K. Artyushkova, J. Gordon, P. Atanassov, A.S. Aricò, V. Baglio, High Performance and Cost-Effective Direct Methanol Fuel Cells: Fe-N-C Methanol-Tolerant Oxygen Reduction Reaction Catalysts, ChemSusChem. 9 (2016) 1986–1995. doi:10.1002/cssc.201600583.

[47] A.H.A. Monteverde Videla, D. Sebastián, N.S. Vasile, L. Osmieri, A.S. Aricò, V. Baglio, S. Specchia, Performance analysis of Fe–N–C catalyst for DMFC cathodes: Effect of water saturation in the cathodic catalyst layer, Int. J. Hydrogen Energy. 41 (2016) 22605–22618. doi:10.1016/j.ijhydene.2016.06.060.

[48] E. Antolini, Effect of the structural characteristics of binary Pt-Ru and ternary Pt-Ru-M fuel cell catalysts on the activity of ethanol electrooxidation in acid medium, ChemSusChem. 6 (2013) 966–73. doi:10.1002/cssc.201300138.

[49] W.J. Zhou, S.Q. Song, W.Z. Li, Z.H. Zhou, G.Q. Sun, Q. Xin, S. Douvartzides, P. Tsiakaras, Direct ethanol fuel cells based on PtSn anodes: the effect of Sn content on the fuel cell performance, J. Power Sources. 140 (2005) 50–58. doi:10.1016/j.jpowsour.2004.08.003.

[50] S. Song, P. Tsiakaras, Recent progress in direct ethanol proton exchange membrane fuel cells (DE-PEMFCs), Appl. Catal. B Environ. 63 (2006) 187–193. doi:10.1016/j.apcatb.2005.09.018.

[51] A.S.A.S. Aricò, D. Sebastian, M. Schuster, B. Bauer, C. D'Urso, F. Lufrano, V. Baglio, C. D'Urso, F. Lufrano, V. Baglio, Selectivity of direct methanol fuel cell membranes, Membranes (Basel). 5 (2015) 793–809. doi:10.3390/membranes5040793.

[52] N. Nakagawa, Y. Kaneda, M. Wagatsuma, T. Tsujiguchi, Product distribution and the reaction kinetics at the anode of direct ethanol fuel cell with Pt/C, PtRu/C and PtRuRh/C, J. Power Sources. 199 (2012) 103–109. doi:10.1016/j.jpowsour.2011.10.057.

[53] Q. Wang, G.Q. Sun, L. Cao, L.H. Jiang, G.X. Wang, S.L. Wang, S.H. Yang, Q. Xin, High performance direct ethanol fuel cell with double-layered anode catalyst layer, 2008. doi:10.1016/j.jpowsour.2007.11.040.

[54] S.C. Zignani, V. Baglio, J.J. Linares, G. Monforte, E.R. Gonzalez, A.S. Aricò, Performance and selectivity of PtxSn/C electro-catalysts for ethanol oxidation prepared by reduction with

different formic acid concentrations, Electrochim. Acta. 70 (2012) 255–265. doi:10.1016/j.electacta.2012.03.055.

[55] S. Rousseau, C. Coutanceau, C. Lamy, J.-M. Léger, Direct ethanol fuel cell (DEFC): Electrical performances and reaction products distribution under operating conditions with different platinum-based anodes, J. Power Sources. 158 (2006) 18–24. doi:10.1016/j.jpowsour.2005.08.027.

[56] A. Serov, M.J. Workman, K. Artyushkova, P. Atanassov, G. McCool, S. McKinney, H. Romero, B. Halevi, T. Stephenson, Highly stable precious metal-free cathode catalyst for fuel cell application, J. Power Sources. 327 (2016) 557–564. doi:10.1016/j.jpowsour.2016.07.087.

[57] P. Piela, C. Eickes, E. Brosha, F. Garzon, P. Zelenay, Ruthenium Crossover in Direct Methanol Fuel Cell with Pt-Ru Black Anode, J. Electrochem. Soc. 151 (2004) A2053. doi:10.1149/1.1814472.